Kapil Garg
Department of Mechanical Engineering,
Indian Institute of Technology Ropar,
Rupnagar 140001, Punjab, India
e-mail: kapil.garg@iitrpr.ac.in

Akshay Rathore
Department of Mechanical Engineering,
Indian Institute of Technology Ropar,
Rupnagar 140001, Punjab, India
e-mail: 2015meb1083@iitrpr.ac.in

Rahul Yadav
Department of Mechanical Engineering,
Indian Institute of Technology Ropar,
Rupnagar 140001, Punjab, India
e-mail: 2015meb1103@iitrpr.ac.in

Sarit K. Das[1]
Department of Mechanical Engineering,
Indian Institute of Technology Ropar,
Rupnagar 140001, Punjab, India
e-mail: skdas@iitm.ac.in

Himanshu Tyagi[2]
Department of Mechanical Engineering,
Indian Institute of Technology Ropar,
Rupnagar 140001, Punjab, India
e-mail: himanshu.tyagi@iitrpr.ac.in

Thermodynamic Analysis of the Volumetric Absorption Solar Collector-Driven Direct Contact Membrane Distillation System

Solar-powered membrane distillation (SP-MD) technology has proven to be an ideal solution for providing fresh water in remote and off-grid locations. In this study, a novel solar energy-driven direct contact membrane distillation (DCMD) cycle is proposed in which a nanofluid-based volumetric absorption solar collector (VASC) is used to drive the DCMD process. The present work focuses on the use of volumetric collector instead of commercially available surface absorption-based solar collector in case of two-loop indirect SP-MD systems, which are installed to control the scaling and corrosion issues in solar collectors. The thermodynamic performance of this two-loop indirect solar-powered DCMD (SP-DCMD) system has been evaluated with the help of a mathematical model prepared in MATLAB. For modeling the DCMD unit, the ε-number of transfer unit (NTU) method used for designing heat exchangers has been employed. The performance of the overall system is evaluated by gained output ratio (GOR), thermal efficiency (η) of the membrane distillation, and water flux (J_w), and effects of various operating parameters related to both DCMD and VASC systems have been understood on the overall system performance. Finally, it has been shown that VASC-driven DCMD system has been approximately 4–15% higher gained output ratio compared to surface absorption-based solar collector (SASC)-driven DCMD system under similar operating conditions.
[DOI: 10.1115/1.4053833]

Keywords: membrane distillation, direct contact, solar energy, nanoparticles-laden fluid, volumetric absorption solar collector, energy systems, heat and mass transfer, thermal systems

1 Introduction

Membrane distillation (MD) has gained much attention in recent years and is a promising technology for purifying highly saline feed streams. It is one of the thermal-based desalination process that separates the fresh water from the saline water (or impure solution) by using a microporous hydrophobic membrane acting as a barrier between the hot saline stream (feed side) and the cold permeate side. Due to the temperature gradient across the MD membrane, there exists a vapor pressure difference across the membrane, resulting in the evaporation of water from the feed side. Only vapors of fresh water pass through the membrane pores and are condensed on the cooler side, and in this way, distillate is obtained [1–4]. This technology offers various advantages in comparison to the other membrane-based technologies such as reverse osmosis: (1) requires lesser pretreatment facilities, (2) can handle highly concentrated feed water (>25%), (3) lesser membrane fouling as membrane is not wetted by water, (4) and since MD membranes have a large pore size, pressure requirements are lower and have tolerance for complete dryout of the membranes [2,3,5–8]. Compared to thermal-based technologies, it is easily scalable and requires a moderate temperature to generate the thermal driving force, and hence, the technology can be coupled with the low-grade heat sources such as waste heat, solar energy, and geothermal energy [5,9–11]. MD technology has several configurations depending on how the vapors are collected from the permeate side. In direct contact membrane distillation (DCMD) configuration, both hot (feed stream) and cold solutions remain in direct contact with the membrane and vapors from the feed side passes through the membrane and gets condensed on the cold solution, which is basically a pure water stream [2,12,13]. In air gap membrane distillation (AGMD), vapors are condensed on a colder surface, which is separated from the membrane by an air gap [2,5]. In sweeping gas membrane distillation, a carrier gas flows through the permeate side, which sweeps the vapor from the permeate side to condense outside the MD module [3,5]. In vacuum membrane distillation (VMD), vacuum is maintained in the permeate side to enhance the pressure difference across the membrane and vapors are condensed outside the MD module [2,3]. The most widely used configurations of MD for desalination are DCMD, AGMD, and VMD. Among all these different configurations of MD, DCMD is considered to be the simplest due to following reasons. It does not require a vacuum pump and external condenser (as in VMD), which makes the initial cost low for a small-scale system, it consumes less electricity and has less membrane pores wetting (as in case of VMD) [3,5,9,12,14,15]. Due to the simplicity and several other benefits of DCMD unit compared to other configurations, and its ability to couple with the solar thermal energy systems, a solar-powered DCMD (SP-DCMD) system is studied in the present work. Such systems can ensure fresh water supply in the remote and off-grid regions in the world, which are economically backward, does not have adequate water supply but having the advantage of higher solar incidence. The SP-DCMD systems can be classified into two broad categories: direct and indirect systems [14]. In direct systems, membrane is an integrated part of the solar collector (may be flat plate, evacuated tube solar collector (ETC), etc.) and feed water is heated inside the MD module. The indirect systems can be further classified into single-loop system and two-loop

[1]Present address: Department of Mechanical Engineering, Indian Institute of Technology Madras, Chennai 600036, Tamil Nadu, India.
[2]Corresponding author.
Manuscript received June 8, 2021; final manuscript received October 28, 2021; published online March 8, 2022. Assoc. Editor: Rui Qiao.

systems. In single-loop SP-DCMD systems, feed water is heated inside the solar collector and then it enters the membrane module, whereas in case of two-loop systems, feed water is heated inside a heat exchanger by a hot fluid stream, which gets heated by absorbing the incident solar energy inside a solar collector. Several researchers have studied these types of systems.

A brief review of those studies is presented here. Elzahaby et al. [12] have investigated the DCMD system driven by a vacuum tube solar collector experimentally and numerically for desalination of the salt water using tubular DCMD module. It was observed that the permeate flux increases with the increase in feed temperature, feed water velocity, and membrane length and decreases with the increase in cooling water temperature. The maximum productivity and gained output ratio (GOR) obtained from this system was 40.587 kg/day and 0.624, respectively. The maximum temperature for the feed water was kept limited to 70 °C to avoid the scale formation. Bamasag et al. [14] have proposed an innovative DCMD module to desalinate aqueous NaCl solution that focuses on directly utilizing the solar thermal energy to heat the feed water by integrating hollow fiber membranes inside an ETC to achieve a more compact system. It was observed that with the membrane having less thickness, water flux through the membrane was higher which happens due to low mass transfer resistance. Finally, it was concluded that under the same operating conditions, by applying solar radiation, water flux and efficiency of the system improve when compared to the case of no radiation and the maximum temperature of the feed water was kept till 65 °C. Similar type of system was also studied by Li et al. [16], where MD modules were directly built into the evacuated solar tubes, and it was concluded that for a feed temperature range of 50–70 °C, system achieved 4–10 L/m^2 h of permeate flux. Chen and Ho [17] have investigated a DCMD system equipped with a solar absorber in which a solar absorber is inserted between the glass cover and feed water channel, which will be heated by the conduction and convection heat transfer between absorber plate and feed water. The system operates in the temperature range of 35–50 °C and produces 4.1 kg/m^2 h of high purity flux. Shim et al. [9] have also investigated the solar-driven DCMD system for seawater desalination by preparing a 2D flat-plate dynamic model with heat and mass transfer mechanisms, and results of the model were found to be in good agreement with experimental results. A flat-plate solar collector was used as a heat source, and thermal energy was supplied to feed water through a heat exchanger (made from titanium) and system gained output ratio ranged from 0.44 to 0.70. Gonazález et al. [4] have also reviewed the different MD systems powered by solar energy, geothermal energy, and waste heat, or hybrid systems that focuses on achieving sustainable desalination.

From the review of the various studies on SP-DCMD systems, it has been observed that the use of surface absorption-based solar collectors (SASC; flat plate, evacuated tube, etc.) has been widely explored to drive the DCMD operation for desalination of saline water. However, due to the high salinity of feed water/seawater (35–55 g/L), the maximum temperature of the feed water is kept low (around 70 °C) to eliminate the deposition of scale forming components on the metallic parts of these collectors. The precipitation of the scaling components (in case of high-feed stream temperature) or keeping the lower operating temperature (to reduce scale formation) reduces the overall thermal performance of the desalination system [18]. A heat exchanger can be used to couple the solar collector and DCMD system such that the feed stream is heated inside the heat exchanger, which eliminates the scaling, fouling, and corrosion of solar collector. Scaling will occur on the metallic parts (heat transfer surfaces) of the heat exchanger, which can be cleaned easily. But adding the heat exchanger will ultimately reduce the overall thermal performance of the desalination system due to addition of one extra component. To address this issue, Garg et al. [19,20] in their recent publications have advised the use of volumetric absorption solar collector (VASC) instead of SASC for multi-stage flash and humidification–dehumidification desalination systems because in volumetric absorption solar collector, there are no metallic parts that eliminates the risk of scaling of solar collectors due to high salinity seawater or high total dissolved solids in feed water. These collectors also offer various other advantages such as relatively 5–10% higher thermal efficiency compared to the SASCs, allow high flux density as there is no absorber plate that otherwise may get damaged due to high flux density, and reduce heat transfer losses in case of high-temperature operation. However, a separate heat exchanger is still required if the DCMD system or any other thermal desalination system is driven by a VASC as nanoparticles are required to be added into a suitable heat transfer fluid such as de-ionized water, glycols, and silicon oil to make it directly absorb the solar energy while flowing through the VASC, and hence, the thermal energy gained by the nanofluid is transferred to the feed water with the help of a heat exchanger. So it can be concluded that if a heat exchanger is used with a SASC to drive the DCMD system, then this system is similar to the DCMD system driven by a VASC, but nanofluid-based solar collector-based DCMD system may have better thermal performance as thermal performance of VASC is higher compared to the thermal performance of the SASC due to which overall performance of the VASC-based DCMD system may improve. In addition, there is no limitation on the operating temperature and flux density for VASCs, which offers an advantage to achieve higher feed water temperature, and thus, higher thermal efficiency of the fresh water production from the DCMD system can be achieved along with eliminating the issue of scaling of solar thermal collectors. At higher feed water temperature, both thermal performance and the distillate production rate are higher.

In the present study, a novel DCMD cycle has been studied, which is driven by a nanofluid-based VASC with the help of a mathematical model as the VASCs have never been employed to drive the MD process, or a parametric study related to the thermal performance of VASC-driven MD process is still not available in the literature despite the several advantages of VASCs for thermal desalination as mentioned earlier. The present study is important to understand the thermal performance of the overall cycle (VASC-based DCMD system) with respect to various important parameters related to both VASC and DCMD systems. Such models help to evaluate the limit of the thermodynamic performance of the combined system as a function of important input parameters and also help in off-designing the system. The mathematical model for VASC is solved using the finite difference implicit method (FDM) [19–21], and for DCMD, a simplified model based on the ε-number of transfer unit (NTU) method is used for the heat exchangers as the operation of DCMD resembles the heat exchanger. Both the mathematical models are solved in MATLAB and are combined to evaluate the thermal performance of the overall system evaluated in terms of GOR and thermal efficiency (η) of the membrane distillation. These mathematical models are also validated with the existing models in the literature. The effect of various important parameters such as particle volume fraction of nanoparticles within the working fluid (f_v), thickness of the working fluid layer inside VASC (H), mass flowrate of working fluid ($\dot{m}_{nf}$), and intensity of solar irradiance incident on the collector ($\dot{q}_{solar}$) are studied on overall system performance measured in terms of GOR, thermal efficiency (η) of the membrane distillation, and permeate flux through the membrane (J_w). Also, the effect of feed water salinity (S) and the length of the membrane module (L) have been evaluated on the permeate flux and GOR of the present system. Finally, the performance of the VASC-driven DCMD system has been compared with the SASC-driven DCMD system on the basis of GOR and permeate flux through the membrane (J_w).

2 Theoretical Modeling

2.1 System Description. Figure 1 shows the schematic of the VASC-driven DCMD system. A counter-flow heat exchanger is employed to transfer the solar thermal energy absorbed by the

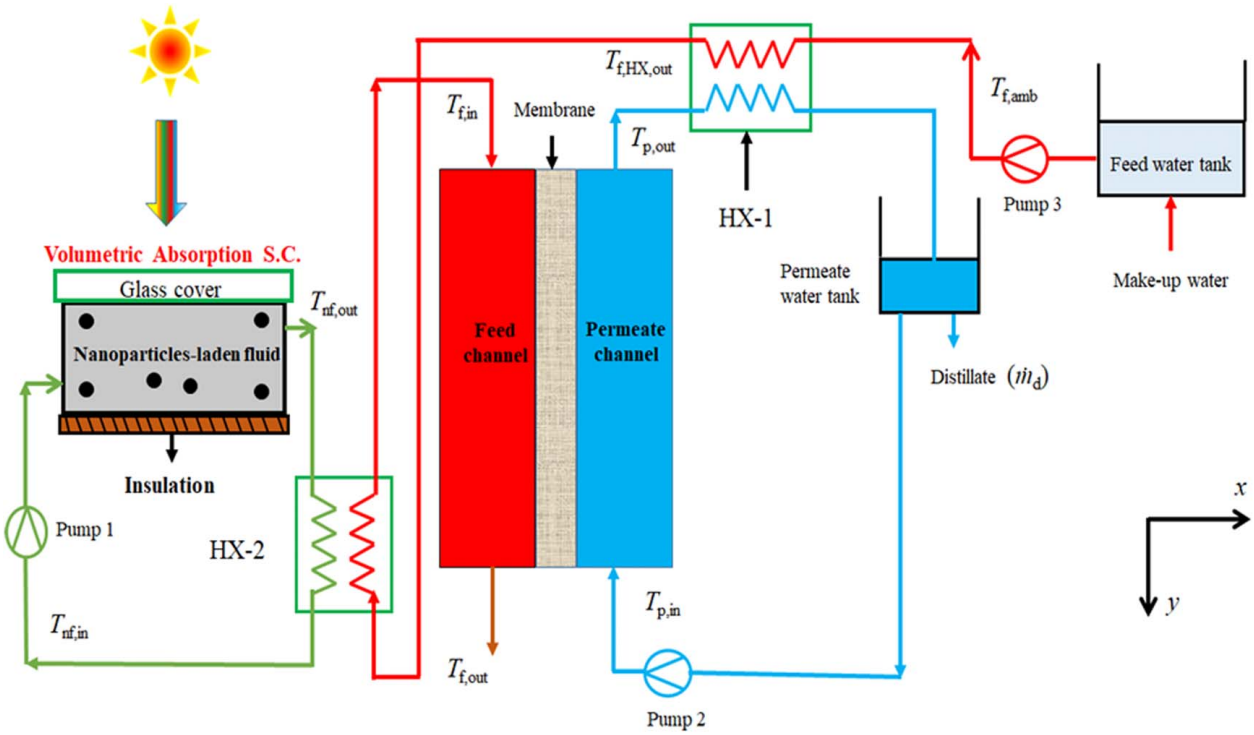

Fig. 1 Schematic of the VASC-driven DCMD system (two-loop indirect solar-powered system)

nanoparticle-laden fluid (inside VASC) to heat the feed water ($\dot{m}_{f,in}$) to a desired temperature, $T_{f,in}$, before it enters the DCMD module. In the present case, a VASC consists of a rectangular channel whose bottom wall is highly insulated. A glass cover ($\tau = 0.98$) is placed at the top of this channel, which allows most of the incident radiation to pass through it and reduces the convective heat transfer losses between the fluid and the ambient. The nanoparticle-laden fluid, which is capable of directly absorbing the entire incident solar energy, consists of amorphous carbon nanoparticles ($d_{np} =$ 10 nm) dispersed in the de-ionized water (base fluid), and it flows in a closed loop between the VASC and the counter-flow heat exchanger. The feed water with mass flowrate $\dot{m}_{f,in}$ and temperature $T_{f,in}$ and pure liquid water (coolant) with mass flow rate $\dot{m}_{p,in}$ and temperature $T_{p,in}$ enter the DCMD module and flows through the feed channel and permeate channels, respectively, and fresh water vapors are transported from the feed side to the permeate side due to the difference in water vapor pressure across the membrane, and the remaining feed water ($\dot{m}_{f,out}$, $T_{f,out}$) is rejected out of the system. The water vapors are condensed on the pure liquid water flowing through the permeate channel due to which it will leave the permeate channel at a relatively higher temperature ($T_{p,out}$). A heat exchanger has been employed to recover the enthalpy of vaporization absorbed by the liquid flowing through the permeate channel, and this energy is transferred to the feed water, which is initially at the ambient conditions ($T_{f,amb}$). Hence, heat energy supplied to the feed water inside the HX-2 can be recovered, which may increase the thermal performance of the overall system.

2.2 Modeling Details of Volumetric Absorption Solar Collector. This section focuses on the mathematical modeling of VASC, which explains the mechanism of conversion of the solar irradiance into thermal energy of nanoparticle-laden fluid (working fluid) flowing through the VASC. The modeling of the VASC done in this study is similar to the one performed in our earlier works [19–21], and the reader is referred to those studies for full details. A concise summary of the same is provided in this section.

As shown in Fig. 1, within the VASC, the incident solar energy directly interacts with the working fluid that either gets absorbed or scattered as it transverse through the finite thickness of the working fluid in the rectangular channel, and finally, solar irradiance absorbed gets converted into the thermal energy in the fluid [10,22]. Scattering of incident radiation is approximated as independent scattering (Rayleigh scattering regime) as (a) very low-volume fractions of nanoparticles ($f_v = 160 \times 10^{-6}$) are used in the present work and (b) the diameter of the nanoparticles (d_{np}) used is very small compared to the wavelength of the incident radiation [21]. A simplified form of the radiative transfer equation (RTE) is used to estimate the attenuation (absorption) of solar irradiance as it transverse through the nanoparticle-laden fluid thickness inside VASC. This simplified version of RTE is called Beer Lambert law by Eq. (1) [19,20,23]:

$$\frac{\partial I_\lambda}{\partial y} = -K_{e\lambda,nf} I_\lambda \tag{1}$$

where $K_{e\lambda}$ is the spectral extinction coefficient for the nanoparticle-laden fluid, y is the thickness of the fluid layer inside VASC, and I_λ is the spectral intensity of the solar radiation incident on the solar collector. In the present study, it is assumed that the incident intensity, which is considered to be the incoming solar radiation, does not get attenuated by atmospheric absorption, and hence, the intensity of incident solar radiation can be calculated using the blackbody relation given by Eq. (2) [24]:

$$I_{b\lambda}(\lambda, T) = \frac{2hc_o^2}{\lambda^5 \left[\exp\left(\frac{hc_o}{\lambda k_B T_{solar}}\right) - 1\right]} \tag{2}$$

where h ($= 6.6256 \times 10^{-34}$ J s) is Planck's constant, k_B ($=1.38 \times 10^{-23}$ J/K) is the Boltzmann constant, c_o ($=2.9979 \times 10^8$ m/s) is the speed of light in the vacuum, λ is the wavelength, and the value of T_{solar} is taken as 5800 K. The extinction in the intensity of incident radiation takes place due to its absorption and scattering by nanoparticles and only absorption by the base fluid. Hence, spectral extinction coefficient for nanoparticle-laden fluid can be

expressed mathematically by the Eq. (3) [21,25]:

$$K_{e\lambda,nf} = \frac{12\pi f_v}{\lambda} \mathrm{Im}\left\{\frac{m^2-1}{m^2+2}\left[1+\frac{\pi^2 d_{np}^2}{15\lambda^2}\left(\frac{m^2-1}{m^2+1}\right)\frac{m^4+27m^2+38}{2m^3+3}\right]\right\} + \frac{8\pi^4 d_{np}^3 f_v}{\lambda^4}\left|\frac{m^2-1}{m^2+2}\right|^2 + \frac{4\pi\kappa_{\lambda,bf}}{\lambda}(1-f_v) \quad (3)$$

where $\kappa_{\lambda,bf}$ is the spectral index of absorption for base fluid and m is the normalized refractive index of the nanoparticles. Values of the optical constants for amorphous carbon nanoparticles and de-ionized water (base fluid) are obtained from Ref. [26].

To obtain the temperature profile within the nanoparticle-laden fluid or to calculate its temperature at the collector outlet ($T_{out,nf}$), a two-dimensional steady-state energy balance equation is solved and is expressed as follows [21,27,28]:

$$k\frac{\partial^2 T}{\partial y^2} - \frac{\partial q_r}{\partial y} = \rho C_p V \frac{\partial T}{\partial x} \quad (4)$$

where k is the thermal conductivity, ρ is the density, C_p is the specific heat capacity of the nanofluid, and V is the velocity of the nanoparticle-laden fluid, which is assumed to be independent of x and y directions as flow of the fluid through the collector is considered to be a slug flow, i.e., a uniform velocity profile is assumed, q_r represents the energy generation term or radiative flux absorbed by the working fluid, which is calculated by Eq. (5) [28]:

$$q_r = \iint I_\lambda d\omega d\lambda \quad (5)$$

Finally, to solve the governing energy balance equation for VASC to obtain the outlet temperature of the working fluid, following boundary conditions are required, which are given as follows [19,20,28,29]:

$$y = 0,\ x > 0,\ h_{conv}[T_\infty - T(x,0)] = -k\left.\frac{\partial T(x,y)}{\partial y}\right|_{y=0} \quad (6)$$

$$y = H,\ x > 0,\ -k\left.\frac{\partial T}{\partial y}\right|_{y=H} = 0 \quad (7)$$

$$x = 0,\ 0 < y < L,\ T(0,y) = T_{nf,in} \quad (8)$$

$$y = 0,\ 0 < x < L,\ I_\lambda(x,0) = \tau I_{b\lambda}(T_{solar}) \quad (9)$$

where y corresponds to the thickness of the working fluid layer ($0 < y < H$) inside VASC, h_{conv} is the convective heat transfer coefficient, and x corresponds to the length of the VASC ($0 < x < L$). Finally, after obtaining the collector outlet temperature, thermal efficiency of the direct absorption solar collector (DASC) can be calculated and is given by Eq. (10):

$$\eta = \frac{\dot{m}_{nf} C_p (T_{nf,out} - T_{nf,in})}{A_c \dot{q}_{solar}} \quad (10)$$

where $\dot{m}_{nf}$ is the mass flowrate of nanofluid, A_c is the top surface area of the collector, and $\dot{q}_{solar}$ is the solar flux incident on the top surface of the collector.

2.3 Mathematical Modeling of Direct Contact Membrane Distillation Unit. A simplified heat exchanger-based mathematical model developed by Swaminathan et al. [30] is used to evaluate the thermal performance of the DCMD unit instead of preparing a numerical model in which the membrane module area is discretized into various cells where the transport equations are solved for these cells, and it is ensured that mass, momentum, and energy are balanced between the cells. This type of model is complicated and is also computationally expensive. The details of the simplified model for the DCMD system used in the present work are provided in Sec. 2.3.1.

2.3.1 Heat and Mass Transfer Process in DCMD System. Heat transfer occurring in the DCMD module has been divided into three parts: (1) heat transfer due to convection across the thermal boundary layer on the feed side ($\dot{q}_f$), (2) heat transfer through the MD membrane ($\dot{q}_m$), which is the sum of heat transfer due to conduction through the membrane ($\dot{q}_{m,cond}$) and due to migration of water vapors through membrane pores ($\dot{q}_{m,mass}$), and (3) convection heat transfer through the thermal boundary layer on the permeate side ($\dot{q}_p$). Figure 2 shows all these heat transfer processes through the DCMD module, which can also be expressed mathematically and are shown below by Eqs. (11)–(13) [1,2,31,32]:

$$\dot{q}_f = h_f(T_{bf} - T_{mf}) \quad (11)$$

$$\dot{q}_m = \dot{q}_{m,cond} + \dot{q}_{m,mass} = h_m(T_{mf} - T_{mp}) + J_w h_{fg} \quad (12)$$

$$\dot{q}_p = h_p(T_{mp} - T_{bp}) \quad (13)$$

where h_f and h_p are the heat transfer coefficients for the feed and permeate boundary layers, respectively, T_{bf} and T_{bp} are the bulk

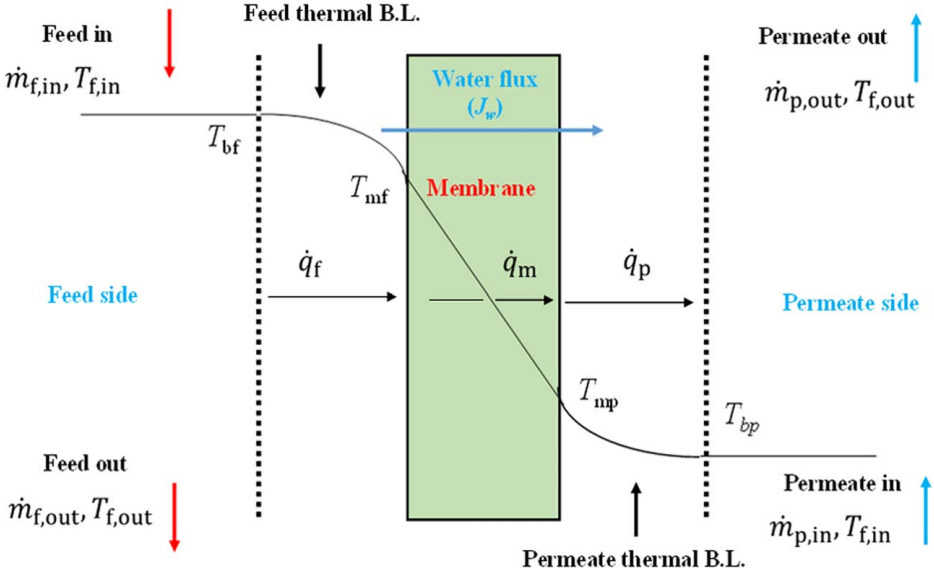

Fig. 2 Heat and mass transfer processes in the DCMD module

feed and permeate temperatures, T_{mf} and T_{mp} are the feed/membrane and permeate/membrane interface temperatures, respectively, h_m is the membrane heat transfer coefficient, J_w is the amount of permeate flux obtained from DCMD module, and h_{fg} is the enthalpy of vaporization of permeate flux.

At steady state, the overall heat transfer flux through the DCMD module (Q) can be expressed as follows:

$$\dot{q} = \dot{q}_f = \dot{q}_m = \dot{q}_p \tag{14}$$

Combining Eqs. (11)–(13), the overall heat flux can be written as follows:

$$\dot{q} = U(T_{bf} - T_{bp}) \tag{15}$$

where U is the overall heat transfer coefficient for the DCMD process and is given by Eq. (16) [1]:

$$\frac{1}{U} = \frac{1}{h_f} + \frac{1}{h_{effc,m}} + \frac{1}{h_c} \tag{16}$$

where $h_{effc,m}$ is the effective heat transfer coefficient of the membrane, which can be expressed as the summation of two resistances in parallel such as (a) resistance offered by the membrane due to heat conduction (δ_m/k_m) and (b) resistance due to mass transfer ($1/h_m^{mass}$) and can be calculated by Eq. (17) [30]:

$$h_{effc,m} = \frac{k_m}{\delta_m} + h_m^{mass} \tag{17}$$

The effective heat transfer coefficient of the membrane ($h_{effc,m}$) is calculated by Eq. (18) [30]:

$$h_{effc,m} = MT_{coeff}\, B h_{fg} + \frac{k_m}{\delta_m} \tag{18}$$

where B is known as membrane permeability and MT_{coeff} is the membrane transfer coefficient and is calculated by Eq. (19) [30]:

$$MT_{coeff} = bA\exp(bT_{p,avg})\left(1 - \frac{BPE}{\Delta T_m}\right) \times \left(\frac{\exp(b(\Delta T_m - BPE)) - 1}{b(\Delta T_m - BPE)}\right) \tag{19}$$

where A (=1054.8) and b (=0.0479) are the fitting parameters for exponential fit of the relation $p_{vap} = Ae^{bT}$, where p_{vap} is the partial pressure of the water vapor, T is expressed in °C, BPE is the boiling point elevation, ΔT_m is the average temperature difference across the membrane, and $T_{p,avg}$ is calculated using Eq. (20) [30]:

$$T_{p,avg} = 0.3586T_{f,in} + 21.922 \tag{20}$$

where $T_{f,in}$ is the temperature of feed water at the inlet of the MD module. The heat transfer coefficients for feed and permeate boundary layers (h_f and h_p) are evaluated by using the correlations given in Eqs. (21) and (22) [1]:

$$h = \left(\frac{k_f}{d_h}\right)0.023\mathrm{Re}^{0.8}\mathrm{Pr}^{0.33} \tag{21}$$

$$h = \left(\frac{k_f}{d_h}\right)0.332\mathrm{Re}^{0.5}\mathrm{Pr}^{0.33} \tag{22}$$

where k_f is the thermal conductivity of the fluid, d_h is the hydraulic diameter, Re is the Reynold number, and Pr is the Prandtl number for the flow of the liquid in both feed and permeate channels. For the turbulent flow in the channels, Eq. (20) is used to obtain the heat transfer coefficients (h_f and h_p), and for laminar flow, Eq. (21) is used. Finally, after calculating the overall heat transfer coefficient (U), effectiveness of the membrane distillation process (ε) is evaluated by assuming the DCMD system a perfect counter-flow heat exchanger and is given by Eq. (23):

$$\varepsilon = \frac{NTU}{1 + NTU} \tag{23}$$

$$NTU = \frac{UA}{C_{min}} \tag{24}$$

where A is the total area of the membrane module and C_{min} is the minimum heat capacity rate of the fluid streams flowing through the membrane module. Finally, the thermal performance of the overall system is evaluated by GOR, which is calculated using Eq. (25) [30]:

$$GOR = \eta \frac{\varepsilon}{1 - \varepsilon} TTD_{factor} \tag{25}$$

where thermal efficiency of the membrane distillation (η) is evaluated using Eq. (26) [30]:

$$\eta = \frac{1}{1 + \left(\left(\frac{K_{cond}}{Bh_{fg}}\right)\left(\frac{1}{MT_{coeff}}\right)\right)} \tag{26}$$

and TTD_{factor} is calculated using Eq. (27) [30]:

$$TTD_{factor} = \frac{TTD}{TTD + TTD_{HX-1}} \tag{27}$$

where TTD is the terminal temperature difference in the membrane distillation module and is calculated using Eq. (28) [30]:

$$TTD = (1 - \varepsilon)\Delta T_{total} \tag{28}$$

where ΔT_{total} is the total temperature difference in the DCMD module, which is the difference between the inlet temperature of feed and permeate streams in the DCMD module. In the present model, both average temperature differences in the DCMD module (ΔT_m) and TTD are unknown, and hence, to calculate both these quantities, Eqs. (28) and (29) [30] are solved simultaneously.

$$\frac{TTD}{\frac{1}{U}} = \frac{\Delta T_m}{\frac{1}{h_{effc,m}}} \tag{29}$$

The terminal temperature difference (TTD_{HX-1}) across the heat exchanger used to recover the distillate energy is calculated using Eq. (30) [30]:

$$TTD_{HX-2} = (1 - \varepsilon_{HX-1})\Delta T_{total,HX-1} \tag{30}$$

where ε_{HX-1} is the effectiveness of the HX-1 calculated using Eq. (23) and $\Delta T_{total,HX-1}$ is the total temperature difference across the HX-1 and is calculated using Eqs. (31) and (32) [30]:

$$\Delta T_{total,HX-1} = T_{f,in} - TTD - T_{P,in} \tag{31}$$

$$T_{p,in} = T_{f,amb} + TTD_{HX-1} \tag{32}$$

where $T_{p,in}$ is the temperature of the permeate stream at the inlet of the membrane module and $T_{f,amb}$ is the temperature of the feed stream at the inlet of the HX-1. The permeate flux (J_w) obtained from the system is also an important parameter to interest to evaluate the performance of the DCMD system and is given by Eq. (33) [30]:

$$J_w = \frac{\dot{m}_d \times 3600}{A} \tag{33}$$

where $\dot{m}_d$ is the mass flowrate of the distillate obtained from the DCMD system and is calculated using Eq. (34) [30]:

$$\dot{m}_d = \frac{(GOR)\dot{Q}_{in}}{h_{fg}} \tag{34}$$

where $\dot{q}_{in}$ is the total heat energy supplied to the feed water in HX-2 and is calculated by Eq. (35) [30]:

$$\dot{Q}_{in} = \dot{m}_f C_{p,f}(TTD + TTD_{HX-1}) \tag{35}$$

3 Results and Discussion

This section deals with the thermal performance of the VASC-driven DCMD system evaluated in the form of GOR and thermal efficiency of the membrane distillation (η). The permeate flux through the membrane (J_w) is an important parameter, which is also analyzed in the present work. Mathematical models are prepared for both VASC and DCMD systems and coupled with each other to calculate the GOR, thermal efficiency (η), and permeate flux (J_w). The mathematical model for VASC is solved in MATLAB using the FDM in which the fluid domain is discretized into x and y directions, resulting into the uniform rectangular elements. Full details related to the procedure for obtaining the governing energy balance Eq. (4) for the volumetric solar collector and the numerical solution for this equation can be obtained from the study by Garg et al. [19]. The working fluid for VASC is assumed to be made of amorphous carbon nanoparticles suspended in the de-ionized water. This fluid is chosen due to its highest solar weighted absorptivity at even very small nanoparticle volume fractions [20,33,34]. Table 1 presents the values of the various input parameters for VASC, which are used to carry out numerical calculations. The mathematical model for direct contact membrane desalination is also prepared, and it is solved in MATLAB. Table 2 presents the values of the various input parameters for DCMD module. All the results in the present study are obtained by the input parameters presented in Tables 1 and 2. To calculate the performance parameters for the present system, the mathematical models for both VASC and DCMD systems are coupled together. The first step is to calculate the collector outlet temperature using the input parameters presented in Table 1, and then by using the simple energy balance equation applied over the counter-flow heat exchanger, the temperature of the feed water at the outlet of the heat exchanger is calculated. For calculating this temperature, the temperature of the feed water at the outlet of the HX-1 is required, which is calculated iteratively. The final step is to calculate the GOR and thermal efficiency of the membrane distillation unit for the input parameters presented in Table 2. The thermal performance of the VASC-driven DCMD system is studied as a function of various important parameters related to both solar collector and DCMD module.

Table 1 Values of the various input parameters for VASC [21,23,33,35]

Input variables	Values
Mass flowrate of nanofluid, $\dot{m}_{nf}$	0.01 kg/s
Surface area of VASC, A_c	4 m^2
Inlet temperature of nanoparticle-laden ?>fluid to VASC, $T_{nf,in}$	25 °C
Convection heat transfer coefficient, h_{conv}	6.5 W/m^2K
Effectiveness of heat exchanger, ε	0.85
Ambient temperature, T_{amb}	25 °C
Material of nanoparticles used for working fluid	Amorphous carbon (C)
Type of base fluid used for working fluid	De-?A3B2 h 0,14ionized water
Mean diameter of nanoparticles used	10 nm
Intensity of solar irradiation	1000 W/m^2

Table 2 Values of the various input parameters used for DCMD module [5,30,36]

Input variables	Values
Mass flowrate of feed water, $\dot{m}_{f,in}$	0.02 kg/s
Mass flowrate of permeate water, $\dot{m}_{p,in}$	0.02 kg/s
Feed water inlet temperature, $T_{bf,a}$	25 °C
Membrane distillation coefficient, B_m	10×10^{-7} kg/m^2Pa s
Membrane material	Millipore ISEQ00010 PVDF
Length of the module, L_m	1 m
Width of the module, W_m	1 m
Flow channel depth, Z_m	1 mm

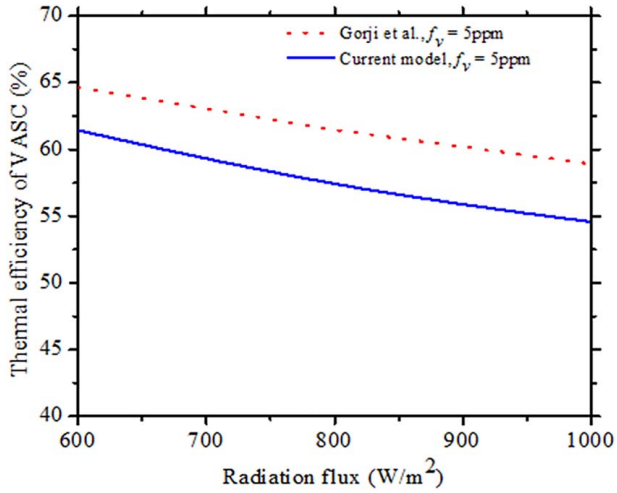

Fig. 3 Results of the validation of the mathematical model for VASC with the model presented by Gorji and Ranjbar [23]

3.1 Validation of the Mathematical Models for VASC and DCMD System. The mathematical models prepared for the VASC and DCMD systems in the present work have been validated individually with the existing mathematical models in the literature. Figure 3 shows the results for the validation of the mathematical model for VASC prepared in the present work with the results of the study by Gorji and Ranjbar [23]. Both these models are solved numerically, and their results are in closer agreement with each other (as shown in Fig. 3) for the same input parameters such as dimensions of the collector, type of working fluid, and incident solar energy. It can also be observed from Fig. 3 that as the solar radiation flux incident on the collector is increased from 600 to 100 W/m^2, the thermal efficiency of VASC decreases. This is due to the fact that when the incident flux on the collector increases, the temperature of the top layer of the working fluid will be higher due to increased absorption of incident energy, and hence, there will be an increase in the convective and radiative heat transfer losses from the top layer to the ambient, and therefore, the overall thermal efficiency of VASC will decrease. But the overall temperature of the working fluid will be higher [23].

The mathematical model prepared for DCMD module in the present work has also been validated with the results of the study by Swaminathan et al. [30], and validation results are shown in Fig. 4, where the effect of channel heat transfer coefficients (h_f and h_p) have been evaluated on (a) gained output ratio and (b) permeate flux (J_w) obtained from the DCMD module and is quantified as liters/m^2/h. It is observed from Fig. 4 that results of both the models are in close agreement with each other and can be used to study the thermal performance of the DCMD system coupled with the volumetric absorption collector. To calculate the NTUs for HX-1, the value of overall heat transfer coefficient was taken as 1300 W/m^2K [30], and total surface area is assumed to be

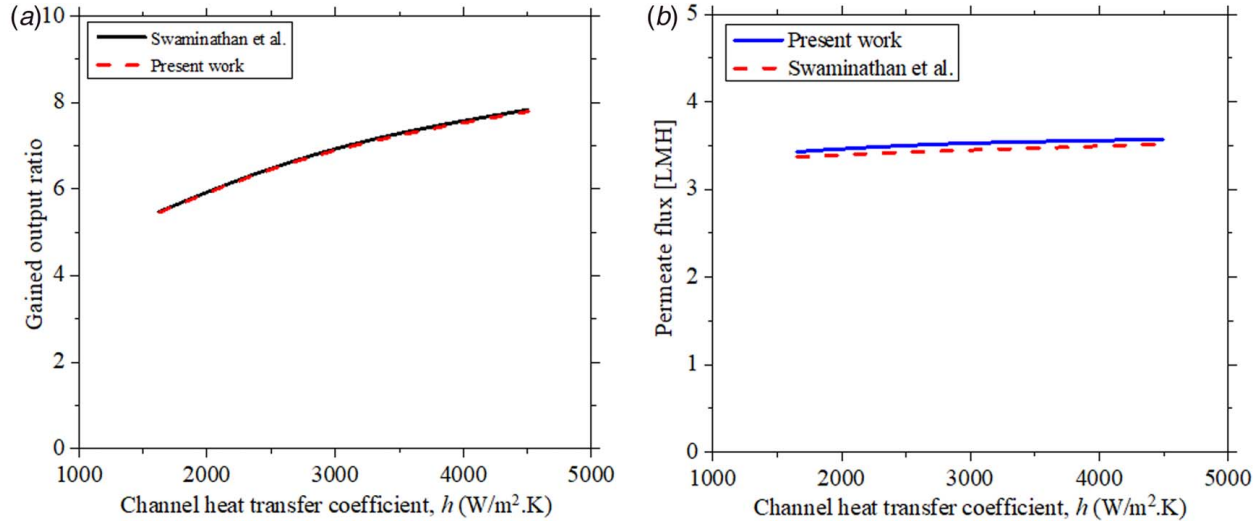

Fig. 4 Results of the validation of the mathematical model for DCMD module presented in terms of (*a*) GOR and (*b*) permeate flux as a function of channel heat transfer coefficient (*h*)

equal to that of area of the membrane module (the same values are also used to evaluate other results in the present work).

3.2 Variation of Collector Outlet Temperature ($T_{nf,out}$) With Respect to Various Parameters Related to VASC. The temperature of nanoparticle-laden fluid (working fluid) at the outlet of the VASC is affected by the amount of nanoparticles added in the base fluid (f_v), thickness of the fluid layer inside the collector (H), mass flowrate of the working fluid ($\dot{m}_{nf}$), and intensity of the incident solar energy on the collector ($\dot{q}_{solar}$) and is shown in Fig. 5. With the increase in the particle volume fraction, the collector outlet temperature increases upto a certain limit, and then it starts decreasing with a further increase in the amount of nanoparticles inside the base fluid. For a certain thickness of the nanofluid layer inside the volumetric absorption solar collector, with an increase in nanoparticle volume fraction, the solar energy absorption capability of the working fluid increases due to increased absorption of the incident radiation by the nanoparticles. This appears as the gain in thermal energy of the nanofluid due to which overall fluid temperature increases. But when the volume fraction is further increased, the incident radiation is trapped only within the top layers of the nanofluid and is unable to reach to the bottom layers of the nanofluid, and hence, the overall fluid temperature decreases. Furthermore, when the irradiation is absorbed within the top layers of the nanofluid, the heat transfer losses from the top fluid layer to the ambient also increases due to the high temperature of the top layer. This phenomenon has been commonly studied by many researchers [10,37].

Similar trend has been observed when the thickness of the nanofluid (working fluid) layer inside VASC is increased for a fixed amount of nanoparticle volume fraction ($f_v = 40 \times 10^{-6}$) as initially there is an increase in the collector outlet temperature with an increase in fluid layer thickness, and later, the increase in collector outlet temperature shows an asymptotic behavior with the increasing fluid layer thickness. This is due to the reason that when the fluid layer thickness is increased from 2 mm to 10 mm, the amount of solar irradiation attenuated within the nanofluid layers increases due to increased absorption of the incident energy by the nanofluid, which increases the overall fluid temperature. But at larger values of the fluid layer thickness, almost entire incident energy gets absorbed within the top layers of the fluid and hence unable to reach to the bottom layers, and as a result, the increase in the overall fluid temperature is almost negligible as shown in Fig. 5(*b*).

The effect of mass flowrate of nanoparticle-laden fluid ($\dot{m}_{nf}$) on collector outlet temperature ($T_{nf,out}$) is also shown in Fig. 5. The mass flowrate of nanofluid is increased by increasing the flow velocity (V) of the nanofluid through the collector, and it can be observed that the increase in mass flowrate leads to reduced collector outlet temperature due to a decrease in the residence time of the nanofluid inside the solar collector as a result of which nanofluid is not able to absorb the entire amount of solar energy incident on the solar collector (DASC). The collector outlet temperature increases with the increase in the incident intensity of the solar radiation as the amount of solar energy absorbed by the nanofluid increases due to which overall fluid temperature becomes higher.

3.3 Effect of Nanoparticle Volume Fraction (f_v) on Gained Output Ratio, Permeate Flux (J_w), and Thermal Efficiency (η) of the Membrane Distillation. The amount of nanoparticles added to the base fluid has a significant effect on the thermal performance of the VASC, which will affect the overall system performance as VASC is the heat source for DCMD in the present work. Hence, it is important to understand its effect on the thermal performance of the overall system. The amount of nanoparticles added to the base fluid is estimated as particle volume fraction (f_v). As shown in Fig. 6, with increase in the particle volume fraction (f_v), temperature of feed water ($T_{f,in}$) to the inlet of the MD module increases rapidly up to a certain amount of volume fraction ($f_v = 40 \times 10^{-6}$), and then, an increase in the volume fraction has almost no effect on the inlet temperature of feed water ($T_{f,in}$). The similar trend can be observed for permeate flux obtained through the membrane (J_w), which increases rapidly with an increase in volume fraction up to $f_v = 40 \times 10^{-6}$, and then, the increase in permeate flux with the increase in volume fraction seems to be negligible. This particular behavior is observed due to the increase in the absorption of the solar irradiance within the working fluid with the increase in the particle volume fraction (volume of particle becomes larger) due to which thermal energy gain in the working fluid increases and its temperature at outlet of the collector ($T_{nf,out}$) will be higher. The working fluid has to transfer the thermal energy to the feed seawater inside a counter-flow heat exchanger, and hence, inlet temperature of feed seawater ($T_{f,in}$) will also be higher due to the higher rate of heat exchange between the two streams inside the heat exchanger. The increase in the inlet temperature of feed water leads to the increase in the water vapor pressure difference across the membrane, and hence, permeate flux passing through the membrane will also increase as

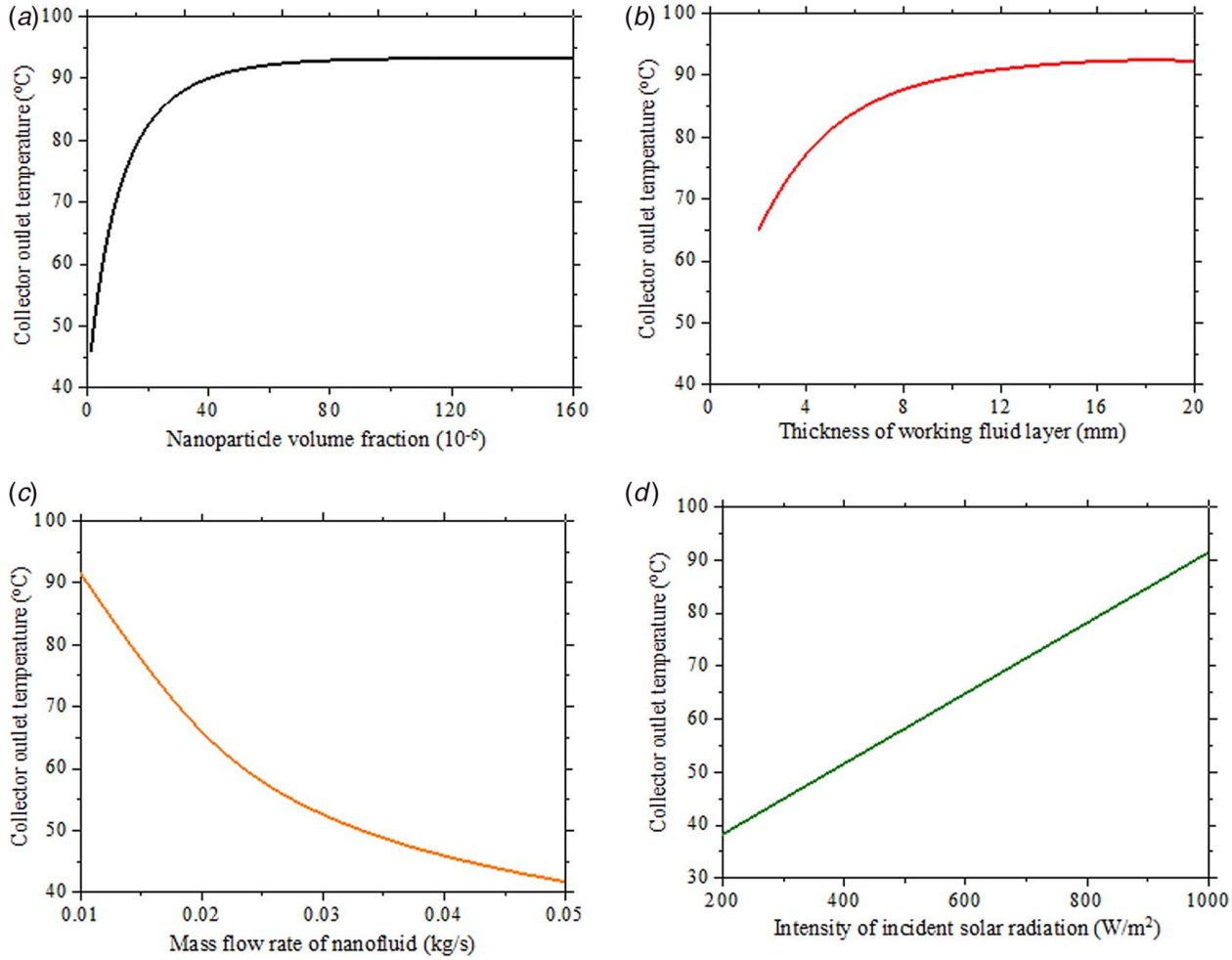

Fig. 5 Effect of (*a*) nanoparticle volume fraction (f_v), (*b*) thickness of working fluid layer (H), (*c*) mass flowrate of nanofluid ($\dot{m}_{nf}$), and (*d*) intensity of incident solar energy ($\dot{q}_{solar}$) on the collector outlet temperature ($T_{nf,out}$)

shown in Fig. 6. But increasing the nanoparticle volume fraction after a certain limit leads to the maximum absorption of solar irradiance within the top layers of the working fluid, which increases the temperature of the top layer, and hence, convective heat transfer losses will also be higher and there was no significant gain in thermal energy. Therefore, the heat transfer rate from the working fluid to feed seawater does not change much and asymptotic behavior of inlet temperature of feed water and permeate flux can be observed within this entire range of particle volume fraction.

The effect of nanoparticle volume fraction on the thermal efficiency (η) of the membrane distillation is shown in Fig. 6, and it can be seen that thermal efficiency also exhibits similar behavior as shown by the permeate flux (J_w). Since thermal efficiency is the ratio of heat transfer due to mass transfer to the total heat transfer through the membrane and hence, by increasing the particle volume fraction (f_v), permeate flux through the membrane increases (as explained earlier) due to which heat transfer also increases, which leads to a higher thermal efficiency. At very higher volume fractions (above $f_v = 40 \times 10^{-6}$), thermal efficiency remains almost same because of negligible change in the permeate flux.

In addition, the effect of particle volume fraction on the GOR of the overall system has also been studied, and it is shown in Fig. 7 that at fixed operating conditions, a change in gained output ratio of the overall system is almost negligible beyond the particle volume fraction of 40×10^{-6}. This is primarily due to the increase in inlet feed water temperature with the increasing particle volume fraction, which results in increase in the permeate flux though the membrane (J_w), and thus, overall performance is higher. The effect of salinity of the feed stream on both permeate flux and gained output ratio is also shown in the same figure (Fig. 7). As salinity of feed water changes, thermophysical properties such as specific heat, density, thermal conductivity, and vapor pressure of the feed water also changes. For numerical calculations, values of these thermophysical properties at different salinities have been obtained from a computer program in MATLAB prepared by Sharqawy et al. [38]. Feed water of four different salinities is taken, and it can be observed that the increase in salinity of the feed stream decrease the permeate flux and GOR of the overall system. This happens due to the decrease in partial pressure of water vapor with the increase in salinity of the feed stream, which decreases the overall vapor pressure difference across the membrane, and hence, both permeate flux and GOR of the system will decrease.

3.4 Effect of Height or Thickness of Working Fluid Layer (H) on Gained Output Ratio (GOR), Thermal Efficiency (η) of the Membrane Distillation and Permeate Flux (J_w).

The height or thickness of nanoparticles-laden fluid (working fluid) flowing through the solar collector is another important parameter which should be taken into consideration. Figures 8 and 9 illustrate the effect of thickness of working fluid layer (H) on permeate flux through the membrane and gained output ratio. By increasing the thickness of working fluid layer, absorption of the solar irradiance within the fluid increases, which increases the working fluid outlet temperature ($T_{nf,out}$) as shown in Fig. 8, which leads to the increase in the permeate flux through the membrane due to higher temperature of feed water at the inlet of the membrane module

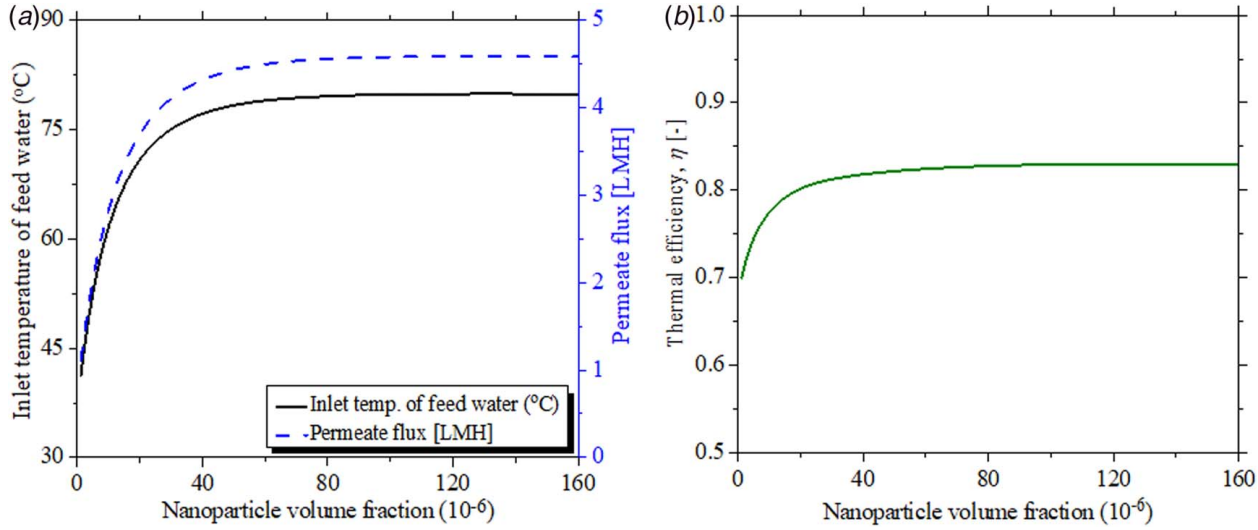

Fig. 6 Effect of nanoparticle volume fraction (f_v) on (*a*) temperature of feed water at the inlet of the MD module ($T_{f,in}$) and permeate flux (J_w) and (*b*) thermal efficiency (η) of the membrane distillation

($T_{f,in}$). The increase in the permeate flux also increases the gained output ratio as shown in Fig. 9. But increasing the thickness of the working fluid layer above $H = 8$ mm is not advantageous because the inlet temperature of feed water ($T_{f,in}$) remains almost the same due to which permeate flux through the membrane and GOR does not change significantly. This happens because at greater thickness of the working fluid layer (at a fixed f_v), the solar irradiance is not able to reach up to the bottom layers and gets absorbed within the top layers due to which the overall outlet temperature of the working fluid does not change significantly. The effect of the length of the membrane module (L) is also shown on the permeate flux (J_w) and GOR of the overall system, which is shown in Fig. 9. Increasing the length of the membrane module increases the gained output ratio but decreases the permeate flux.

The effect of thickness of the working fluid layer on thermal efficiency (η) of the DCMD is same as that of the nanoparticle volume fraction, which is shown by Fig. 8. Increasing the thickness of the working fluid layer increases the inlet temperature of feed water (as shown in Fig. 8), which leads to an increase in the thermal efficiency due to the increased rate of heat transfer due to vapor transport due to higher inlet feed water temperatures ($T_{f,in}$).

3.5 Effect of Mass Flowrate of Nanoparticles-Laden Fluid ($\dot{m}_{nf}$) on Gained Output Ratio and Permeate Flux (J_w). The mass flowrate of nanoparticle-laden fluid (working fluid) inside VASC is an important parameter, and its effect on the thermal performance of the overall system should be studied and results are presented in Fig. 10. In the present calculations, the mass flowrate of the working fluid is increased by increasing the flow velocity. As a result, when the working fluid flows through the collector at higher velocities, the amount of incident energy absorbed (per unit mass) will be reduced due to lesser exposure time under solar irradiation. Consequently, the collector outlet temperature will reduce as explained earlier. Due to the lower collector outlet temperature, the temperature of feed water at the inlet of the MD module will also decrease, which decreases the overall permeate flux through the membrane (J_w) as shown in Fig. 10(*a*).

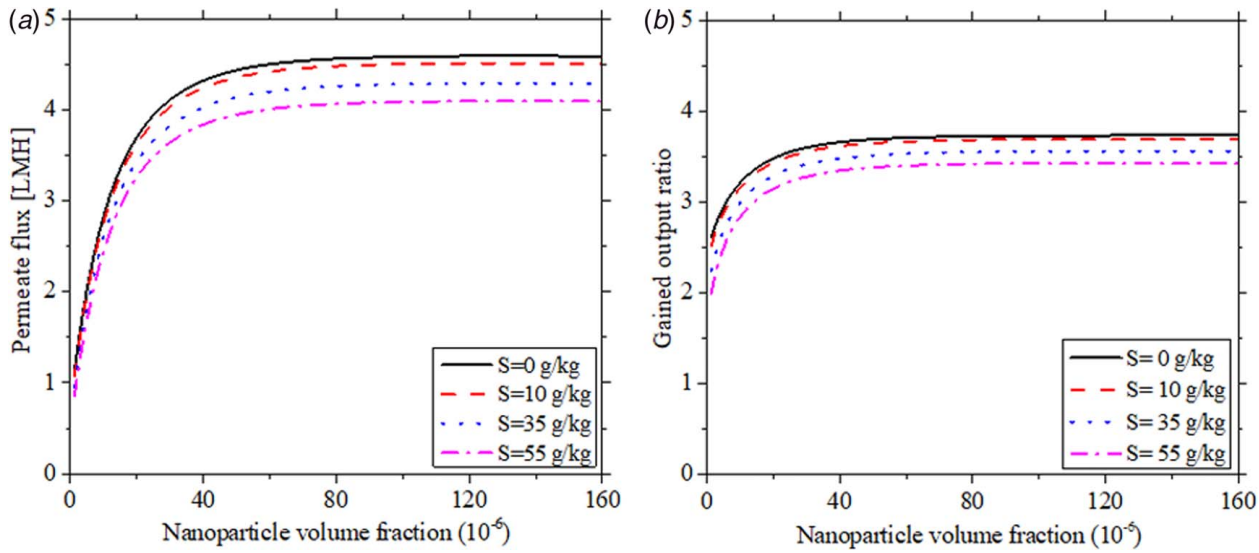

Fig. 7 Effect of nanoparticle volume fraction (f_v) and salinity of the feed stream (S) on (*a*) permeate flux (J_w) and (*b*) GOR of the overall system

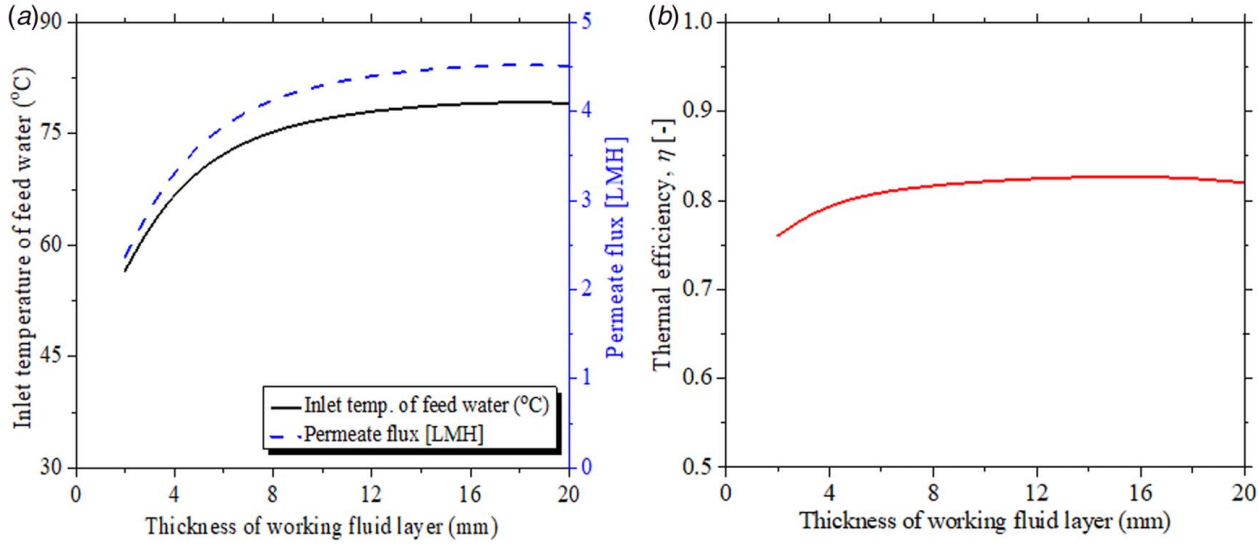

Fig. 8 Effect of thickness of the working fluid layer (*H*) on (*a*) temperature of feed water at the inlet of the MD module ($T_{f,in}$) and permeate flux through the membrane (J_w) and (*b*) thermal efficiency (η) of the membrane distillation

The lowering of permeate flux through the membrane results in lower values of GOR, which is shown in Fig. 10(*b*).

3.6 Effect of Intensity of Incident Solar Energy ($\dot{q}_{solar}$) on Gained Output Ratio and Permeate Flux (J_w). The effect of intensity of incident solar energy ($\dot{q}_{solar}$) on water flux through the membrane (J_w) and GOR is shown in Fig. 11. With the increase in the incident solar irradiance, the solar energy absorbed by the working fluid will also increase, and consequently, its outlet temperature increases. With the increase in the outlet temperature of the working fluid ($T_{nf,out}$), the temperature of feed water at the inlet of the MD module ($T_{f,in}$) will also increase, which increases the permeate flux through the membrane as well as the GOR of the overall system. In the present study, the maximum value for the collector outlet temperature was approximately 93 °C and maximum value of inlet temperature of feed water ($T_{f,in}$) was approximately 72 °C. It can be concluded that by an appropriate selection of working fluid (with base fluid having higher boiling point than deionized water) and by increasing the optical concentration, even greater inlet feed temperatures can be achieved, which will lead to even higher values of GOR.

3.7 Comparison of the VASC-DCMD and SASC-DCMD Systems. This section compares the thermal performance of the VASC- driven DCMD system with the SASC-driven DCMD system. The comparison is done by assuming the similar operating conditions for both these systems such as solar collector working fluid flowrate, solar collector area, ambient conditions, inlet temperature of the working fluid, and intensity of incident solar energy. For comparison, the working fluid for VASC is taken as amorphous carbon-based nanoparticle-laden fluid with nanoparticles volume fraction, $f_v = 40 \times 10^{-6}$, thickness of the fluid layer, $H = 8$ mm, and mean diameter of nanoparticles, $d_{np} = 10$ nm. For SASC, pure water is assumed as the working fluid. The dimensions of the DCMD module, membrane permeability, flowrates of feed water and permeate water, and their inlet temperatures of the

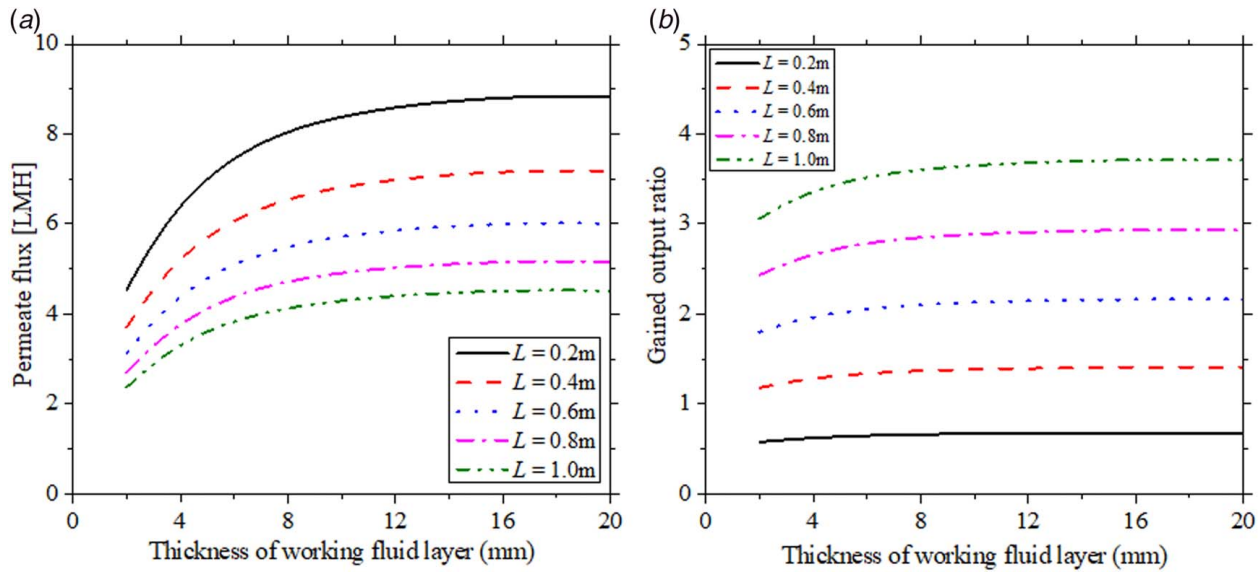

Fig. 9 Effect of the thickness of the working fluid layer (*H*) and length of the membrane module (*L*) on (*a*) permeate flux (J_w) and (*b*) GOR

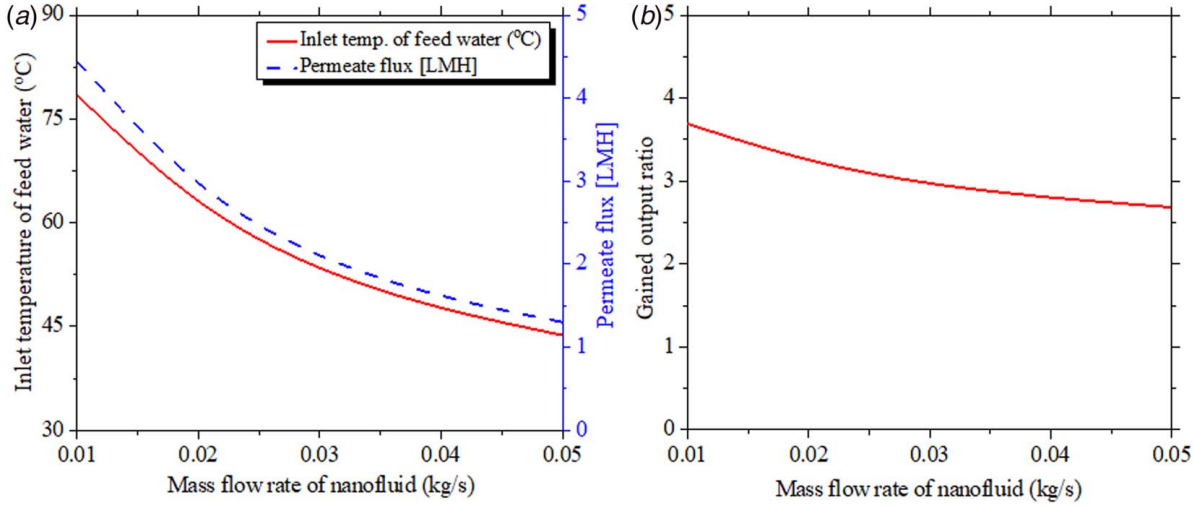

Fig. 10 Effect of mass flowrate of nanofluid ($\dot{m}_{nf}$) on (*a*) permeate flux through the membrane (J_w) temperature of feed water to the inlet of the MD module ($T_{f,in}$) and (*b*) GOR

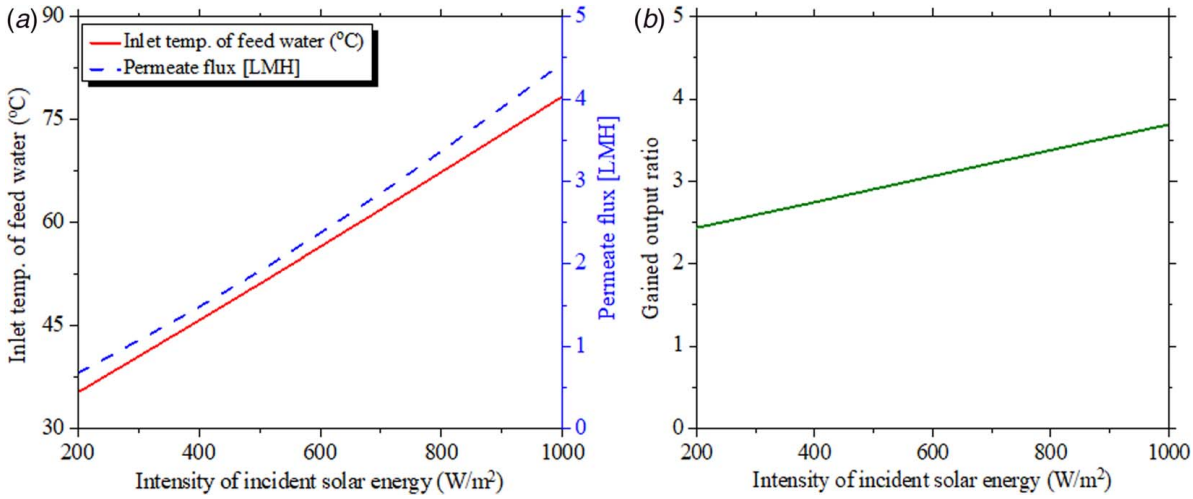

Fig. 11 Effect of intensity of incident solar energy ($\dot{q}_{solar}$) on (*a*) permeate flux through the membrane (J_w) and temperature of feed water at the inlet to the membrane module ($T_{f,in}$) and (*b*) GOR

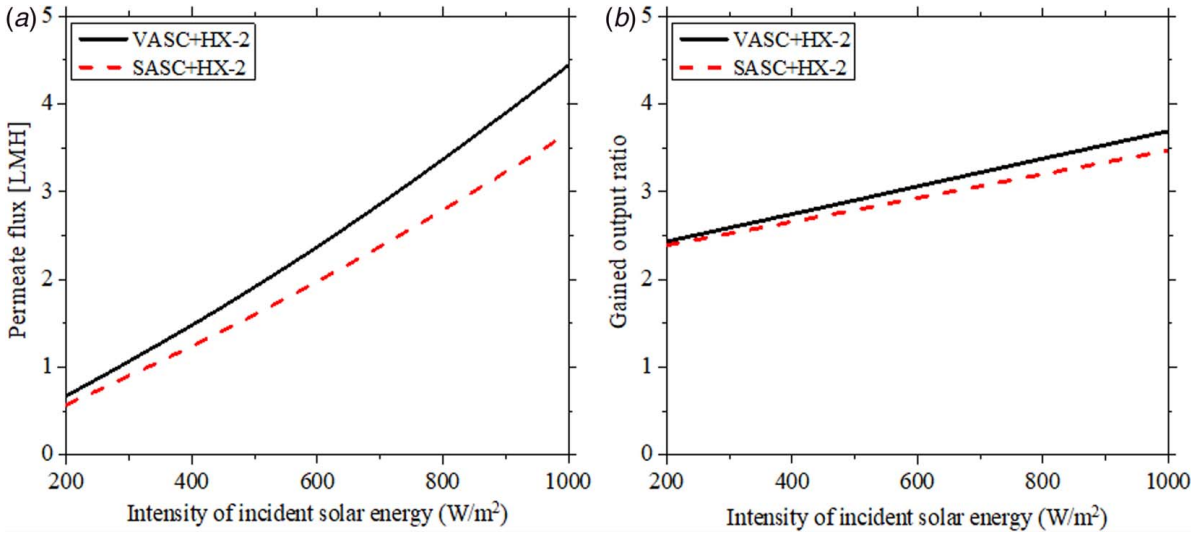

Fig. 12 Comparison of the thermal performance of the VASC-driven DCMD system with SASC-driven DCMD system in terms of (*a*) permeate flux and (*b*) GOR

module are also assumed to be same for both the systems. It is already mentioned that the thermal efficiency of VASC is relatively 5–10% higher compared to that of SASC [34], and hence, from the value of thermal efficiency of VASC obtained for the aforementioned operating conditions, the outlet temperature of the working fluid ($T_{nf,out}$) flowing through SASC is calculated by using the relation for the thermodynamic efficiency of the solar collector, which is $\eta = (T_{nf,out} - T_{nf,in})/A_c \dot{q}_{solar}$, by taking the thermal efficiency of SASC to be 10% less compared to that of VASC. This outlet temperature of the working fluid for SASC ($T_{wf,out}$) is used to calculate the water flux through the membrane (J_w) and GOR of the overall system.

The GOR is evaluated for both the systems as a function of intensity of solar energy incident on the collector ($\dot{q}_{solar}$) as shown in Fig. 12. It can be observed that under similar operating conditions, GOR for VASC-driven DCMD system is relatively 3–17% higher compared to that of SASC-driven DCMD system. The higher GOR for VASC-driven system is due to the relatively higher outlet temperature of the working fluid ($T_{nf,out}$) from VASC due to which the rate of thermal energy exchange between the working fluid and feed water inside the heat exchanger is higher, and hence, the temperature of feed water at inlet to the membrane module ($T_{f,in}$) will be higher for this system. As explained earlier, at higher inlet feed temperatures, the driving force for the water vapors migration through the membrane increases, and consequently, both water flux and GOR will be higher. Figure 12 shows the comparison of the fresh water flux obtained from both the systems.

4 Conclusions

MD has a great potential for desalination of saline water, which can be coupled with renewable energy sources such as solar thermal energy. Being the simplest of all the possible MD configurations, DCMD unit has been studied in the present work. A nanofluid-based VASC, which has relatively higher thermal efficiency s compared to the SASC has been chosen to drive the DCMD operation. A simplified ε-NTU method has been used to model the DCMD unit instead of complex and computationally expensive numerical models. It is shown that the thermal performance of the system shows an asymptotic behavior with respect to nanoparticle volume fraction (f_v) and thickness of the working fluid (H) using input parameters presented in Tables 1 and 2, and thus increasing their values beyond a certain limit is not advantageous in terms of overall thermal performance of the system. The thermal performance decreases with the increasing mass flowrate of nanofluid inside the collector and increases when the incident flux on the collector increases. The increasing salinity of feed water lowers the GOR and the fresh water production rate. There exists a trade-off between GOR and fresh water production rate when the length of the membrane module is increased. Finally, it has been shown that, under identical conditions, VASC-driven DCMD system performs better in terms of water production and gained output ratio. Also, the effects of salinity of feed water and incident solar energy on gained output ratio and water flux have been shown. It can be concluded that to address the reduced thermal performance of the indirect solar-powered DCMD system having two-loop coupling scheme, which is used to control the corrosion and scaling in cheap and commercially available solar collectors, more simple and relatively highly efficient VASC may be used to drive the desalination process via MD.

Acknowledgment

The authors wish to acknowledge the support provided by Department of Mechanical Engineering at Indian Institute of Technology Ropar.

Conflict of Interest

There are no conflicts of interest.

Data Availability Statement

The datasets generated and supporting the findings of this article are obtainable from the corresponding author upon reasonable request. The authors attest that all data for this study are included in the paper. Data provided by a third party listed in Acknowledgment.

Nomenclature

d = mean diameter of nanoparticles (nm)
h = heat transfer coefficient (W/m^2/K)
k = thermal conductivity (W/m/K)
m = normalized refractive index (−)
A = area (m^2)
B = membrane distillation coefficient (kg/m^2/s/Pa)
H = thickness or height of working fluid layer
I = intensity (W/m^2/K^4)
J = permeate flux (kg/m^2/s)
K = extinction coefficient (m)
L = length (m)
S = salinity (g/L)
T = temperature (°C)
U = overall heat transfer coefficient (W/m^2 K)
V = fluid velocity (m/s)
W = width (m)
Z = thickness (m)
$\dot{m}$ = mass flowrate (kg/s)
$\dot{q}$ = heat flux (W/m^2)
d_h = hydraulic diameter (m)
f_v = particle volume fraction (−)
h_{fg} = enthalpy of vaporization (J/kg)
p_{vap} = vapor pressure (Pa)
q_r = radiative flux (W/m^2)
C_p = specific heat capacity (J/kg/K)
$\dot{q}_{in}$ = total heat energy supplied (W)
MT = membrane transfer coefficient (−)
Pr = Prandtl number (−)
Re = Reynolds number (−)

Greek Symbols

δ = membrane thickness
ε = effectiveness
η = thermal efficiency
κ = index of absorption
λ = wavelength
ρ = density
τ = transmissivity
ω = solid angle

Subscripts

amb = ambient
bf = bulk feed
bp = bulk permeate
cond = conductive
d = distillate
e = extinction
f = feed water
in = inlet
m = membrane
mf = feed/membrane interface
mp = permeate/membrane interface

nf = nanoparticles-laden fluid
np = nanoparticle
out = outlet
p = permeate water
solar = solar energy
v = vapor
w = water

References

[1] Qtaishat, M., Matsuura, T., Kruczek, B., and Khayet, M., 2008, "Heat and Mass Transfer Analysis in Direct Contact Membrane Distillation," Desalination, **219**(1–3), pp. 272–292.
[2] Alkhudhiri, A., Darwish, N., and Hilal, N., 2012, "Membrane Distillation: A Comprehensive Review," Desalination, **287**, pp. 2–18.
[3] Ashoor, B. B., Mansour, S., Giwa, A., Dufour, V., and Hasan, S. W., 2016, "Principles and Applications of Direct Contact Membrane Distillation (DCMD): A Comprehensive Review," Desalination, **398**, pp. 222–246.
[4] González, D., Amigo, J., and Suárez, F., 2017, "Membrane Distillation: Perspectives for Sustainable and Improved Desalination," Renewable Sustainable Energy Rev., **80**, pp. 238–259.
[5] Summers, E. K., and Arafat, H. A., 2012, "Energy Efficiency Comparison of Single-Stage Membrane Distillation (MD) Desalination Cycles in Different Configurations," Desalination, **290**, pp. 54–66.
[6] Qtaishat, M. R., and Banat, F., 2013, "Desalination by Solar Powered Membrane Distillation Systems," Desalination, **308**, pp. 186–197.
[7] Lokare, O. R., Tavakkoli, S., Rodriguez, G., Khanna, V., and Vidic, R. D., 2017, "Integrating Membrane Distillation with Waste Heat From Natural Gas Compressor Stations for Produced Water Treatment in Pennsylvania," Desalination, **413**, pp. 144–153.
[8] Shafieian, A., Khiadani, M., and Nosrati, A., 2019, "Performance Analysis of a Thermal-Driven Tubular Direct Contact Membrane Distillation System," Appl. Therm. Eng., **159**, p. 113887.
[9] Shim, W. G., He, K., Gray, S., and Moon, I. S., 2015, "Solar Energy Assisted Direct Contact Membrane Distillation (DCMD) Process for Seawater Desalination," Sep. Purif. Technol., **143**, pp. 94–104.
[10] Bhalla, V., and Tyagi, H., 2018, "Parameters Influencing the Performance of Nanoparticles-Laden Fluid-Based Solar Thermal Collectors: A Review on Optical Properties," Renewable Sustainable Energy Rev., **84**, pp. 12–42.
[11] Sha, A., and Khiadani, M., 2019, "A Novel Solar-Driven Direct Contact Membrane-Based Water Desalination System," Energy Convers. Manage., **199**, p. 112055.
[12] Elzahaby, A. M., Kabeel, A. E., Bassuoni, M. M., Refat, A., and Elbar, A., 2016, "Direct Contact Membrane Water Distillation Assisted With Solar Energy," Energy Convers. Manage., **110**, pp. 397–406.
[13] Kabeel, A. E., Abdelgaied, M., and El-said, E. M. S., 2017, "Study of a Solar-Driven Membrane Distillation System : Evaporative Cooling Effect on Performance Enhancement," Renewable Energy, **106**, pp. 192–200.
[14] Bamasag, A., Alqahtani, T., Sinha, S., Ghaffour, N., and Phelan, P., 2020, "Experimental Investigation of a Solar-Heated Direct Contact Membrane Distillation System Using Evacuated Tube Collectors," Desalination, **487**-(March), p. 114497.
[15] Lisboa, K.M., de Moraes, D.B., Naveira-Cotta, C.P. and Cotta, R.M., 2021, "Analysis of the Membrane Effects on the Energy Efficiency of Water Desalination in a Direct Contact Membrane Distillation (DCMD) System With Heat Recovery," Appl. Therm. Eng., **182**, p. 116063.
[16] Li, Q., Beier, L., Tan, J., Brown, C., Lian, B., Wang, Y., Dai, P., et al., 2019, "An Integrated, Solar-Driven Membrane Distillation System for Water Purification and Energy Generation," Appl. Energy, **237**, pp. 534–548.
[17] Chen, T. C., and Ho, C. D., 2010, "Immediate Assisted Solar Direct Contact Membrane Distillation in Saline Water Desalination," J. Membr. Sci., **358**(1–2), pp. 122–130.
[18] Lienhard, J. H., Antar, M. A., Bilton, A., Blanco, J., and Zaragoza, G., 2012, "Solar Desalination," *Annual Review of Heat Transfer*, Begell House, Danbury, CT, pp. 277–347.
[19] Garg, K., Khullar, V., Das, S. K., and Tyagi, H., 2018, "Performance Evaluation of a Brine-Recirculation Multistage Flash Desalination System Coupled With Nanofluid-Based Direct Absorption Solar Collector," Renewable Energy, **122**, pp. 140–151.
[20] Garg, K., Khullar, V., Das, S. K., and Tyagi, H., 2019, "Parametric Study of the Energy Efficiency of the HDH Desalination Unit Integrated With Nanofluid-Based Solar Collector," J. Therm. Anal. Calorim., **135**(2), pp. 1465–1478.
[21] Tyagi, H., Phelan, P. E., and Prasher, R. S., 2009, "Predicted Efficiency of a Low-Temperature Nanofluid-Based Direct Absorption Solar Collector," ASME J. Sol. Energy, **131**(4), p. 041004.
[22] Ohri, V., and Khullar, V., 2019, "Using Solar Energy for Water Purification Through Nanoparticles Assisted Evaporation," ASME J. Sol. Energy Eng., **141**, p. 011008.
[23] Gorji, T. B., and Ranjbar, A. A., 2016, "A Numerical and Experimental Investigation on the Performance of a Low-Flux Direct Absorption Solar Collector (DASC) Using Graphite, Magnetite and Silver Nanofluids," Sol. Energy, **135**, pp. 493–505.
[24] Incropera, F. P., DeWitt, D. P., Bergman, T. L., and Lavine, A. S., 2007, *Fundamentals of Heat and Mass Transfer*, 6th ed., Wiley India, Noida, India.
[25] Bohren, C. F., and Huffman, D. R., 2008, *Absorption and Scattering of Light by Small Particles*, Wiley, New York.
[26] Palik, E. D., 1997, *Handbook of Optical Constants of Solids, Five-Volume Set: Handbook of Thermo-Optic Coefficients of Optical Materials With Applications*, Elsevier Science, Cambridge, MA.
[27] Otanicar, T. P., Phelan, P. E., Prasher, R. S., Rosengarten, G., and Taylor, R. A., 2010, "Nanofluid-Based Direct Absorption Solar Collector," J. Renewable Sustainable Energy, **2**(3), p. 033102.
[28] Bhalla, V., Khullar, V., and Tyagi, H., 2019, "Investigation of Factors Influencing the Performance of Nanofluid-Based Direct Absorption Solar Collector Using Taguchi Method," J. Therm. Anal. Calorim., **135**(2), pp. 1493–1505.
[29] Phelan, P., Otanicar, T., Taylor, R., and Tyagi, H., 2013, "Trends and Opportunities in Direct-Absorption Solar Thermal Collectors," ASME J. Therm. Sci. Eng. Appl., **5**(2), p. 021003.
[30] Swaminathan, J., Chung, H. W., Warsinger, D. M., and Lienhard V, J. H., 2016, "Membrane Distillation Model Based on Heat Exchanger Theory and Configuration Comparison," Appl. Energy, **184**, pp. 491–505.
[31] Termpiyakul, P., and Jiraratananon, R., 2005, "Heat and Mass Transfer Characteristics of a Direct Contact Membrane Distillation Process for Desalination," Desalination, **177**(1–3), pp. 133–141.
[32] Zuo, G., Wang, R., Field, R., and Fane, A. G., 2011, "Energy Efficiency Evaluation and Economic Analyses of Direct Contact Membrane Distillation System Using Aspen Plus," Desalination, **283**, pp. 237–244.
[33] Garg, K., Khullar, V., Das, S. K., and Tyagi, H., 2018, "Numerical Study of Nanofluid-Based Solar Collector for Humidification-Dehumidification (HDH) Desalination," ASME International Mechanical Engineering Congress and Exposition, Vol. 52088, Pittsburgh, PA, Nov. 9–15, p. V06BT08A032.
[34] Khullar, V., Bhalla, V., and Tyagi, H., 2017, "Potential Heat Transfer Fluids (Nanofluids) for Direct Volumetric Absorption-Based Solar Thermal Systems," ASME J.Therm. Sci. Eng. Appl., **10**(1), p. 011009.
[35] Garg, K., Bhalla, V., Khullar, V., Das, S. K., and Tyagi, H., 2017, "Performance Evaluation of Single Stage Flash Evaporation Desalination System Coupled with Nanofluid-Based Direct," 24th National and 2nd International ISHMT-ASTFE Heat and Mass Transfer Conference (IHMTC-2017), Hyderabad, India, Dec. 27–30, pp. 1–8, Paper No. IHMTC2017-19-0659.
[36] Saffarini, R. B., Summers, E. K., Arafat, H. A., and Lienhard V, J. H., 2012, "Economic Evaluation of Stand-Alone Solar Powered Membrane Distillation Systems," Desalination, **299**, pp. 55–62.
[37] Bhalla, V., Khullar, V., and Tyagi, H., 2018, "Experimental Investigation of Photo-Thermal Analysis of Blended Nanoparticles (Al2O3/CO3O4) for Direct Absorption Solar Thermal Collector," Renewable Energy, **123**, pp. 616–626.
[38] Sharqawy, M. H., Lienhard V, J. H., and Zubair, S. M., 2010, "Thermophysical Properties of Seawater: A Review of Existing Correlations and Data," Desalin. Water Treat., **16**(1–3), pp. 354–380.